Interaction of manganese with single-wall B_2O nanotubes: An *ab initio* study

Guowen Peng,[1] Yuan Ping Feng,[1,*] and Alfred C. H. Huan[2,3]
[1]*Department of Physics, National University of Singapore, 2 Science Drive 3, Singapore 117542*
[2]*Institute of Materials Research and Engineering, 3 Research Link, Singapore 117602*
[3]*Division of Physics and Applied Physics, Nanyang Technological University, 1 Nanyang Walk, Singapore 637616*
(Received 19 November 2005; revised manuscript received 13 March 2006; published 25 April 2006)

Interaction of a manganese atom with a graphitic B_2O sheet and a (3,0) single-wall B_2O nanotube was investigated using first-principles spin-polarized density functional calculations. The stable geometries, electronic and magnetic properties of the Mn-doped planar and tubular systems were analyzed. It was found that the most stable adsorption site is above the hole site for the B_2O sheet. For the (3,0) B_2O nanotube, when the Mn atom is adsorbed outside the tube, the most energetically favorable site is the center of the hexagon with an axial symmetry, followed by the bridge site above the axial B-B bond. The magnetic moment of the Mn-doped nanotube is similar to that of the free Mn atom. The atop oxygen site, however, is the most stable site if the Mn atom is inside the tube. In this case, the Mn atom is seven-coordinated and the nanotube is significantly distorted, leading to a larger binding energy and a smaller magnetic moment of $\sim 1\mu_B$.

DOI: 10.1103/PhysRevB.73.155429 PACS number(s): 61.48.+c, 73.61.Wp, 75.75.+a, 71.15.Nc

I. INTRODUCTION

The study of interaction of transition metal (TM) atoms with nanotubes[1] is of great interest in nanophysics. On one hand, it is important to understand the growth mechanism of nanotubes and the roles played by the TM catalysts during the synthesis.[2–4] On the other hand, it is essential to produce TM-nanotube functional nanodevices, such as nanocontacts, nanowires, metal coated or encapsulating ferromagnetic structures, and nanoelectronic devices.[5–12]

Besides carbon nanotubes, many other tubular sp^2 structures, such as BN, BC_2N, BC_3, $B_xC_yN_z$ nanotubes,[13–16] have been investigated. Recently, B_2O nanotube has been theoretically predicted to be stable.[17] Compared to carbon and BN nanotubes, B_2O has a moderate energy gap which is independent of its chirality. Therefore, B_2O nanotubes may have potential applications in electronic and optical nanodevices. While the planar B_2O has been produced,[18] to our knowledge, the tubular form has not been synthesized yet, even though one would expect that this kind of nanotube could be synthesized via the current methods using TM atoms as catalysts. To explore this possibility and to understand the effect of adsorption of TM atoms on the properties of B_2O nanotubes, it is of great interest to investigate the interaction of TM atoms with single-wall B_2O nanotubes.

In this study, we performed first-principles spin-polarized density functional calculations to investigate the interaction of a manganese atom with a (3,0) single-wall B_2O nanotube. The computational details are given in the next section. In the first part of Sec. III, adsorption of a single Mn atom on the graphitic B_2O sheet is discussed. Results of binding energies, electronic structures, and magnetic properties corresponding to various binding sites are presented. The adsorptions of a single Mn atom at various sites on the outer and inner walls of the (3,0) zigzag single-wall B_2O nanotube are discussed in the second and third parts of Sec. III, respectively. In each case, the structural, electronic, and magnetic properties of the Mn-doped (3,0) single-wall B_2O nanotube are analyzed. A conclusion is given in the last section.

II. COMPUTATIONAL METHOD

Total energy calculations based on spin-polarized density functional theory were performed using VASP code.[19,20] The ultrasoft pseudopotentials[21] were used for electron-ion interactions and the generalized gradient approximation (GGA) of Perdew and Wang[22] was used to describe the exchange-correlation functional. The electron wave function was expanded using plane waves with a cutoff energy of 520 eV.

For the single B_2O sheet, we adopted the model proposed by Zhang and Crespi (ZC)[17] (Fig. 1). Compared to other models, the ZC model has the lowest energy and preserves hexagonal symmetry after relaxation.[18] A supercell containing a 24-atom B_2O layer was used to model the Mn-doped B_2O sheet. A vacuum region of 10 Å thick was used to separate the periodic B_2O sheets. The size of the supercell is $9.054 \times 9.054 \times 10.00$ Å^3. The Brillouin zone was sampled with a $4 \times 4 \times 1$ k-point mesh based on the Monkhorst-Pack scheme.[23] The relaxed lattice constant of the single B_2O sheet is 4.527 Å within GGA. The B-B and B-O bond lengths are 1.545 and 1.494 Å, respectively. The calculated cohesive energy is 6.16 eV/atom. In the optimized single B_2O sheet, an out-of-plane relaxation is observed, resulting in a C_{3v} symmetry of the B_2O sheet. The relative protrusion (the distance between the highest oxygen and the lowest boron atom) is 0.1 Å in our calculation. This, however, is smaller than the value (1.5 a.u.) reported in an earlier local density approximation (LDA) calculation.[17] The energy gap of 1.9 eV obtained in the present calculation is also smaller compared to the value of 2.8 eV obtained in the earlier LDA calculation.[17] We have also optimized the geometry of the single B_2O sheet within LDA and obtained a lattice constant of 4.44 Å which is about 2% smaller than the GGA value. A larger out-of-plane relaxation of 0.40 Å was found and the calculated band gap increased to 2.06 eV. It is known that GGA (LDA) tends to overestimate (underestimate) the lattice constant. The discrepancy in the magnitudes of out-of-plane relaxation of the single B_2O sheet obtained using GGA and

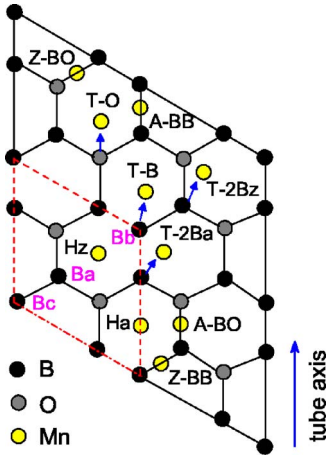

FIG. 1. (Color online) Different adsorption sites for a single Mn atom on the graphitic B_2O sheet and the (3,0) B_2O nanotube. The dashed region indicates the unit cell of the graphitic B_2O sheet. For the B_2O sheet, the axial and zigzag sites are equivalent, namely, $H_a \Leftrightarrow H_z$, T-$2B_a \Leftrightarrow T$-$2B_z$, A-BB $\Leftrightarrow Z$-BB, and A-BO $\Leftrightarrow Z$-BO.

LDA, respectively, could be due to the difference in lattice constants. We checked this possibility by relaxing the atomic positions within GGA but fixed the lattice parameter to the LDA optimized value. As expected, a larger out-of-plane relaxation of 0.60 Å and a wider band gap of 2.62 eV were obtained, confirming that the larger out-of-plane relaxation in the LDA calculations is due to the smaller LDA lattice parameter.

The single-wall (3,0) B_2O nanotube, which is similar in size to the (9,0) single-wall carbon nanotube (SWCNT), was chosen in our study. To minimize the interaction between Mn atoms in neighboring cells, we used a supercell which is two units long in the direction of the tube axis, i.e., 8.833 Å. The lateral dimension of the supercell is 15×15 Å which is sufficient to eliminate interaction between tubes in neighboring cells. We used a $1 \times 1 \times 7$ (Γ included) k-point mesh to sample the Brillouin zone. All structures were fully optimized using the conjugate gradient method until the Hellmann-Feynman forces were less than 0.05 eV/Å. In the optimized nanotube structure, the B-B and B-O bond lengths are among 1.556–1.562 Å and 1.487–1.493 Å, respectively. A significant buckling of 0.473 Å [24] was observed for the relatively weak B-B bonds, which resulted in the small curvature energy of B_2O nanotube, only 0.02 eV/atom in our calculation. The average diameter of the (3,0) B_2O nanotube is 7.45 Å. Compared to the value 1.63 eV in Ref. 17, our calculated energy gap is 1.49 eV for the (3,0) B_2O nanotube.

III. RESULTS AND DISCUSSION

To investigate the interaction of a single Mn atom with the graphitic B_2O sheet, six different adsorption sites were considered (Fig. 1). These include a single Mn atom (i) over the center of a hexagon (H_a or H_z site in Fig. 1), (ii) directly over an oxygen atom (T-O site), (iii) atop a type I boron atom which is bonded to three boron atoms (T-B site), (iv) atop a type II boron atom which has two oxygen atoms and one boron atom as its nearest neighbors (T-$2B_a$ or T-$2B_z$ site), (v) at the bridge site over a B-B bond (A-BB or Z-BB site), and (vi) at the bridge site over a B-O bond (A-BO or Z-BO site).

TABLE I. The calculated binding energies (E_b) and magnetic moments (μ) for different adsorption sites of a single Mn atom on a graphitic B_2O sheet and a (3,0) B_2O nanotube, respectively. Only the stable adsorption sites are listed.

System	Site	E_b (eV)	μ (μ_B)
Sheet	H	1.32	5.00
	BB	1.22	5.00
	BO	1.18	3.02
	T-O	1.02	3.00
	T-B	0.60	3.39
Outer wall of (3,0) tube	H_a	1.70	5.00
	A-BB	1.47	5.00
	H_z	1.37	5.00
	Z-BB	1.28	5.00
	T-O	1.10	3.00
	A-BO	0.85	3.00
Inner wall of (3,0) tube	T-O	1.62	1.00
	Center	0.41	5.00
	A-BB	0.26	5.00
	A-BO	0.15	3.00
	H_a	0.13	5.00

For the Mn-doped (3,0) B_2O nanotube, a bond can be oriented either along the direction of the tube axis (axial direction) or along the zigzag lines around the tube (zigzag direction) and some of the aforementioned adsorption sites become inequivalent. Here H_a refers to the center of the hexagon with an axial symmetry while H_z refers to the center of hexagons with a different orientation. T-$2B_a$ indicates the adsorption site atop a type II boron atom which forms an axial bond with another boron atom, while T-$2B_z$ involves a type II boron atom which forms a zigzag bond with its neighboring boron atom. A-BB and Z-BB refer to the bridge sites over an axial B-B and zigzag B-B bond, respectively. Similarly, A-BO and Z-BO indicate the bridge sites over an axial B-O and zigzag B-O bond, respectively. Since B_2O tube has two surfaces, inside and outside, adsorptions on both sides of the surface were considered. Thus, we considered a total 20 initial adsorption sites for the Mn-doped B_2O nanotube. These different sites are shown in Fig. 1.

For each adsorption site, we fully relaxed the structure and calculated its binding energy and magnetic moment. The results are listed in Table I. The binding energy (E_b) is defined as

$$E_b = E(\text{pure}) + E(\text{Mn}) - E(\text{Mn-doped}), \quad (1)$$

where E(pure) is the total energy of the undoped system (the pure B_2O sheet or the pure B_2O nanotube), E(Mn) is the spin-polarized total energy of a Mn atom in the $3d^5 4s^2$ ground state configuration, and E(Mn-doped) is the spin-

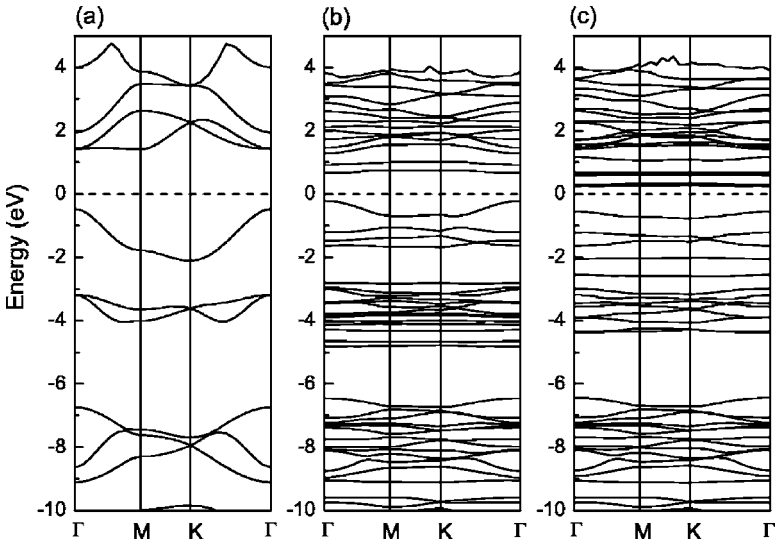

FIG. 2. Band structures of (a) the clean graphitic B_2O sheet; (b) the majority spin, and (c) the minority spin for Mn adsorption at the *H* site on B_2O sheet. The Fermi level is indicated by the dashed line.

polarized total energy of the optimized structure of the Mn-doped system (the Mn-doped B_2O sheet or the Mn-doped B_2O nanotube).

A. Interaction of Mn with the graphitic B_2O sheet

As shown in Table I, the *H* (H_a or H_z) site was found to be most stable among the various adsorption sites considered for the graphitic B_2O sheet, with a binding energy of 1.32 eV. In the optimized structure, the position of Mn is 2.56 Å above the B_2O sheet. Two of the boron atoms (B_a and B_b in Fig. 1) moved towards the Mn atom, through a 0.97 and 0.62 Å out-of-plane relaxation, respectively, resulting in formation of two Mn-B bonds. The bond lengths are 2.22 and 2.36 Å, respectively.

The calculated band structures and local density of states (LDOS) for the *H* configuration of the Mn-doped B_2O sheet are shown in Figs. 2 and 3, respectively. The band structure of the clean graphitic B_2O sheet is also shown in Fig. 2 for comparison. In the majority spin bands [Fig. 2(b)], five bands characteristic of Mn 3*d* orbital are located between 4.0 eV and 4.8 eV below the Fermi level, with small dispersion. Another flat band appears at 2.8 eV below the Fermi level, which corresponds to the Mn 4*s* orbital and boron (B_b) 2*p* orbital, as can be seen from the LDOS (Fig. 3). On the other hand, in the minority spin bands [Fig. 2(c)], a dispersionless band appears at 2.6 eV below the Fermi level, which is due to the mixture of the Mn 4*s* and boron (B_b) 2*p* orbitals. Another nearly flat band appears at 2.0 eV below Fermi level, which is mainly contributed by the 2*p* orbitals of borons (B_a and B_c, see Fig. 1). The total magnetic moment per Mn atom of the Mn-doped graphitic B_2O sheet is almost the same as that of a free Mn atom. Projection of the magnetic moment onto the atomic sites showed that B_a contributes about $-0.1\mu_B$ to the total magnetic moment. A Mulliken charge analysis indicated that there is a small charge transfer from the Mn 4*s* orbital to the 2*p* orbital of B_a.

It is noted that the second most stable configuration, the BB site (*A*-BB or *Z*-BB in Fig. 1), has a binding energy of 1.22 eV, only 0.1 eV smaller than that of the most stable *H* site. In the relaxed BB configuration, the Mn atom moved closer to the type II boron atom. The distances between the Mn atom and the bridge boron atoms are 2.16 and 2.36 Å, respectively. The total magnetic moment of the BB configuration is the same as that of the *H* configuration. The *T*-2B site (*T*-$2B_a$ or *T*-$2B_z$ in Fig. 1) was found unstable and transformed into the BB configuration after structural relaxation.

The remaining three configurations, i.e., *T*-B, *T*-O, and BO (*A*-BO or *Z*-BO in Fig. 1) were also found less stable, as indicated by the smaller binding energies in Table I. They also have lower magnetic moments, about $3\mu_B$. In the optimized *T*-O configuration, the O atom below the Mn was pushed away from its original position in the B_2O sheet by Mn, resulting in its vertical position being 0.73 Å lower than that of its three B neighbors. The distance between this O atom and the Mn is 2.21 Å. A similar analysis, as done for the *H* site, revealed that the effective electronic configura-

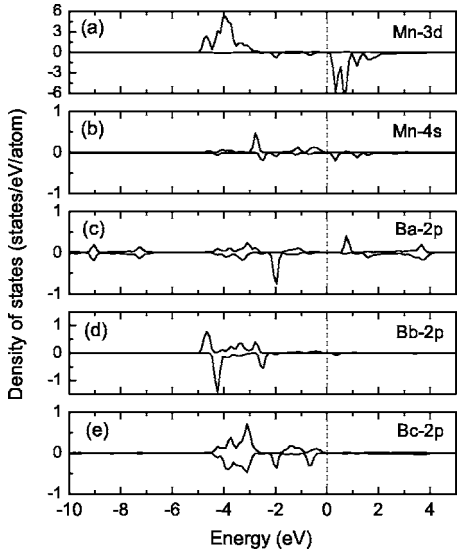

FIG. 3. Projections of local density of states onto (a) the Mn 3*d* orbital, (b) the Mn 4*s* orbital, (c) the B_a 2*p* orbital, (d) the B_b 2*p* orbital, (e) the B_c 2*p* orbital, for Mn adsorption at the *H* site on B_2O sheet. Atoms B_a, B_b, and B_c are labeled in Fig. 1.

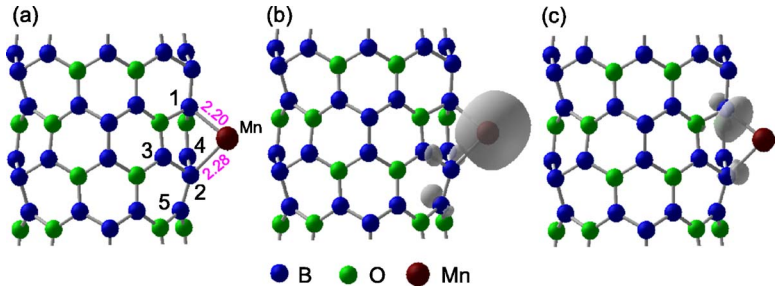

FIG. 4. (Color online). (a) The relaxed structure of the B_2O nanotube with a Mn atom adsorbed at the H_a site. The spin density isosurfaces correspond to (b) 0.02 $e/Å^3$, and (c) −0.01 $e/Å^3$ for the same configuration.

tions of the Mn atom in the *T*-B, *T*-O, and BO sites are close to $3d^74s^0$. The low binding energies of these configurations could be due to the high energy penalty for promoting the 4*s* orbital to the 3*d* orbital.

B. Adsorption of Mn to the outer wall of (3,0) B_2O nanotube

For the B_2O nanotube, in principle, the Mn atom can be attached to either inside or outside of the tube wall. Both cases were considered in our study. In the case of outside adsorption, the H_a site was found energetically most favorable, with a binding energy of 1.70 eV, followed by the *A*-BB site with a binding energy of 1.47 eV. The other hole site, H_z, however, is only 0.1 eV less stable than the second most favorable *A*-BB site. Both H_a and H_z configurations show high magnetic moments, $5\mu_B$ per Mn. Metastable H_a and H_z configurations with low magnetic moments ($3\mu_B$ per Mn) were also found in our calculations. The binding energies of these states are 1.32 and 0.90 eV, respectively. The *Z*-BB site is also quite stable, with a binding energy of 1.28 eV, very close to that of the H_z site. Adsorptions at the *T*-$2B_z$ and *Z*-BO site were unstable and both transformed to the *Z*-BB configuration after structural relaxation. Similarly, the initial configurations with Mn adsorbed at the *T*-B and *T*-$2B_a$ sites both relaxed to the *A*-BB configuration. It is interesting to note that in the optimized *T*-O configuration, the Mn atom pushed the oxygen atom below inward by 1.18 Å from its position in the pure B_2O tube.

In the relaxed H_a configuration [Fig. 4(a)], the distances between the Mn atom and its two nearest neighboring boron atoms [atoms 1 and 2 in Fig. 4(a)] are 2.20 and 2.28 Å, respectively, very close to those in the *H* configuration of the Mn-doped B_2O sheet. The calculated band structure and LDOS for the H_a configuration are shown in Figs. 5 and 6, respectively. The energy band diagram of the pure (3,0) B_2O tube is also shown in Fig. 5(a) for comparison. In the band structure of majority spin [Fig. 5(b)], five Mn 3*d* bands are clearly visible between 3.0 and 4.8 eV below the Fermi level [Fig. 6(a)]. One Mn 4*s* band lies at 3.0 eV below the Fermi level. Similarly, one Mn 4*s* band is clearly seen at 3.0 eV below the Fermi level in the minority spin. However, there is no Mn 3*d* band in the valence bands of minority spin. Figure 4(b) shows the spin density isosurface corresponding to 0.02 $e/Å^3$ for the H_a configuration of Mn-doped (3,0) B_2O tube. It shows that boron atoms 3, 4, and 5 [Fig. 4(a)] have finite positive spin densities, with 0.02, 0.02, and $0.03\mu_B$ local magnetic moments, respectively. On the contrary, the two axial boron atoms which are nearest neighbors of Mn [atoms 1 and 2 in Fig. 4(a)] have negative spin densities, as shown in Fig. 4(c). Notice that the local magnetic moment ($-0.10\mu_B$) of boron atom 1 is very large, which comes mainly from its 2*p* orbitals, as clearly shown by the LDOS [Fig. 6(d)].

C. Adsorption of Mn to the inner wall of (3,0) B_2O nanotube

For adsorption on the inside wall of the nanotube, it is interesting to note that the initial H_z, *T*-B, *Z*-BB, *Z*-BO, and *A*-BB configurations all relaxed to the same structure which is indicated by *A*-BB in Table I. In this optimized structure,

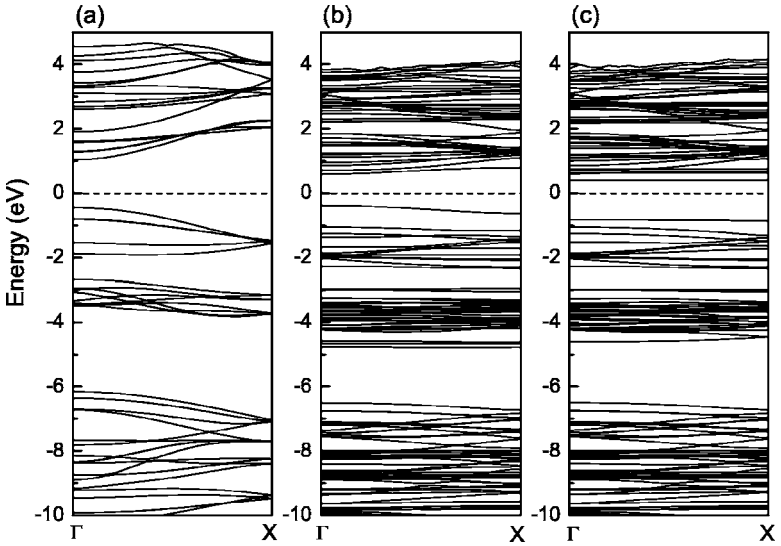

FIG. 5. Band structures of (a) the pure (3,0) B_2O nanotube; (b) the majority spin, and (c) the minority spin of Mn adsorption at the H_a site on the outer wall of the (3,0) B_2O nanotube. The Fermi level is indicated by the dashed line.

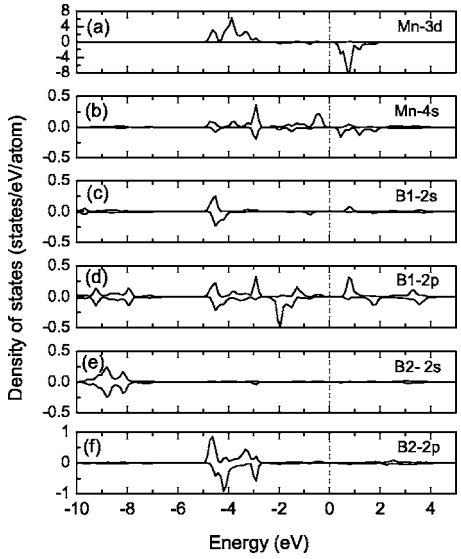

FIG. 6. Projections of local density of states onto (a) the Mn 3*d* orbital, (b) the Mn 4*s* orbital, (c) the 2*s* orbital, and (d) the 2*p* orbital of boron atom 1, (e) the 2*s* orbital, and (f) the 2*p* of boron atom 2, for Mn adsorption at the H_a site on the outer wall of the (3.0) B_2O nanotube. Boron atoms 1 and 2 are shown in Fig. 4(a).

the Mn atom is left encapsulated inside the tube without chemically bonding to any atoms, as shown in Fig. 7. This is similar to the equilibrium structure when a substitutional catalytic Ni atom in a SWCNT is spontaneously replaced by a nearby C atom.[3] The distances between the Mn atom and the two closest neighbors, the axial bridge boron atoms, are 2.34 and 2.58 Å, respectively, both are larger than the summation of the covalent radii of Mn atom (1.39 Å) and B atom (0.82 Å). The lower binding energy (0.26 eV) implies that the Mn atom is physisorbed on the B_2O nanotube. As a result, the magnetic moment of the Mn-doped system in these configurations is exactly the same as that of a free Mn atom. For adsorption at the *T*-2B_a or *T*-2B_z site, it was found that the Mn atom was relaxed almost to the center of the tube, without bonding to any atoms. This configuration (indicated by "Center" in Table I) is slightly more stable than the *A*-BB configuration.

The most stable adsorption site on the inner wall of the nanotube is *T*-O, as shown by the large binding energy in Table I. In the optimized structure [Fig. 8(a)], the Mn atom pushed outward the oxygen atom next to it [atom 4 in Fig.

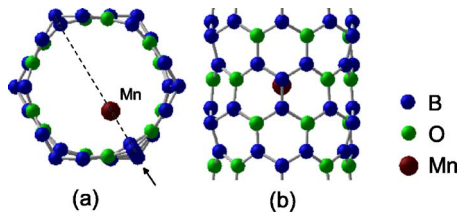

FIG. 7. (Color online) Top view (a) and side view (b) [along the direction indicated by the arrow in (a)] of the relaxed (3,0) B_2O nanotube with a Mn atom adsorbed at *A*-BB, where the Mn atom is encapsulated inside the tube without chemically bonding to any atoms.

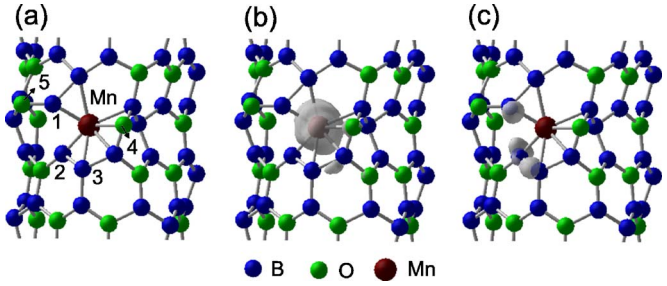

FIG. 8. (Color online) (a) The relaxed structure of the (3,0) B_2O nanotube with a Mn atom adsorbed at the *T*-O site inside the tube wall. The spin density isosurfaces corresponding to (b) 0.015 $e/Å^3$, and (c) −0.025 $e/Å^3$, respectively, for the same configuration.

8(a)] and another oxygen atom nearby [atom 5 in Fig. 8(a)], by 1.34 and 1.41 Å, respectively, and the two oxygen atoms ended up at the bridge sites above boron atoms. The seven-coordinated Mn atom is almost in the tube wall and occupies the original position of oxygen atom 4. As a result, the B_2O nanotube is severely distorted. Considering also the relaxed structures of Mn adsorption at the *T*-O sites of the B_2O graphitic sheet and the outer wall of the (3,0) B_2O nanotube, there seems a general trend: Mn tends to push the oxygen atom out of the plane or the tube wall so that it can form more bonds with B atoms. As a matter of fact, this is also true for the *T*-B site. In the relaxed *T*-B configuration of Mn adsorbed on the B_2O sheet, the boron atom underneath Mn was also pushed out of the plane but by a smaller amount compared to the oxygen atom in the *T*-O site, which could be due to different strengths of the B-B and B-O bonds. In the case of Mn adsorption to the outer wall of the nanotube, the situation is slightly different due to the curvature of the tube wall. The BB site (*A*-BB or *Z*-BB) is a stable adsorption site and Mn simply took the easy way and relaxed to this site. This tendency of Mn preferring large coordination leads to the significant deformation of the B_2O nanotube when Mn is adsorbed to the inner wall of the nanotube.

Due to the large coordination and interaction with the neighboring oxygen atom, the Mn in the *T*-O configuration

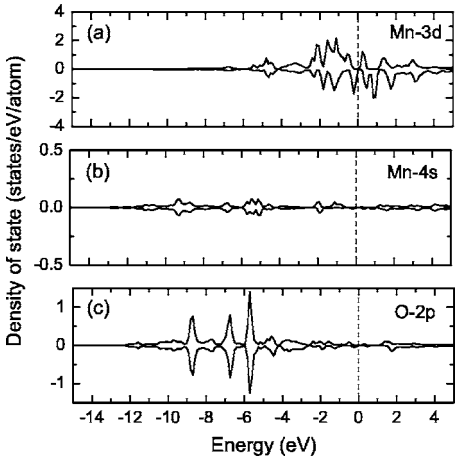

FIG. 9. The projected local density of states onto (a) the Mn 3*d* orbital; (b) the Mn 4*s* orbital, and (c) the 2*p* orbital of the oxygen atom which is bonded to the Mn atom for a single Mn atom adsorbed at the *T*-O site inside the (3,0) B_2O nanotube.

inside the nanotube shows different LDOS (Fig. 9). It can be seen in Fig. 9 that bonds are formed from the two Mn 4*s* electrons and two 2*p* electrons of the neighboring oxygen atom. The Mn 3*d* electrons are delocalized and their densities are broadened. About 3.34 *e* and 2.07 *e* occupy the spin-up and spin-down channels of the Mn 3*d* orbitals, respectively. As a result, the total magnetic moment of the doped system is very small, only $1\mu_B$. Figures 8(b) and 8(c) show the spin density isosurfaces corresponding to 0.015 and $-0.025\ e/\text{Å}^3$, respectively, for the *T*-O configuration of the Mn-doped (3,0) B_2O tube. As seen in Fig. 8(c), three of the boron atoms surrounding Mn [atoms 1, 2, and 3 in Fig. 8(a)] have significant negative spin densities, with local magnetic moments of −0.04, −0.05, and $-0.03\mu_B$, respectively. On the other hand, the oxygen atom bonded to the Mn atom has positive spin density [Fig. 8(b)], with $0.01\mu_B$ local magnetic moment. The local magnetic moment of the Mn atom is $1.23\mu_B$. Contributions from all atoms result in a total magnetic moment of $1\mu_B$ for the Mn-doped tube system.

IV. CONCLUSIONS

In conclusion, a systematic investigation on the interaction of a Mn atom with a graphitic B_2O sheet and a single-wall zigzag (3,0) B_2O nanotube was presented. For the Mn-doped B_2O sheet, the most stable adsorption site is the *H* site. For adsorption of a single Mn atom on the outer wall of the (3,0) B_2O nanotube, the most energetically favorable site is the H_a site, followed by the *A*-BB site, with the total magnetic moment equivalent to that of a free Mn atom. On the other hand, the *T*-O site is the most stable adsorption site inside the nanotube, with a low magnetic moment of $1\mu_B$. In the relaxed *T*-O configuration, the B_2O nanotube is significantly distorted due to adsorption of the Mn atom. Further studies of the interactions of other TM atoms, such as Fe, Co, Ni, with B_2O nanotubes will be useful to fully understand the binding trends and in exploring potential applications.

*Electronic address: phyfyp@nus.edu.sg

[1] S. Iijima, Nature (London) **354**, 56 (1991); S. Iijima and T. Ichihashi, *ibid.* **363**, 603 (1993).
[2] Y. H. Lee, S. G. Kim, and D. Tománek, Phys. Rev. Lett. **78**, 2393 (1997).
[3] A. N. Andriotis, M. Menon, and G. Froudakis, Phys. Rev. Lett. **85**, 3193 (2000).
[4] F. Banhart, J.-C. Charlier, and P. M. Ajayan, Phys. Rev. Lett. **84**, 686 (2000).
[5] C. K. Yang, J. Zhao, and J. P. Lu, Phys. Rev. Lett. **90**, 257203 (2003).
[6] D. M. Duffy and J. A. Blackman, Phys. Rev. B **58**, 7443 (1998).
[7] M. Menon, A. N. Andriotis, and G. E. Froudakis, Chem. Phys. Lett. **320**, 425 (2000).
[8] C. Binns, S. H. Baker, A. M. Keen, S. N. Mozley, C. Norris, H. S. Derbyshire, and S. C. Bayliss, Phys. Rev. B **53**, 7451 (1996).
[9] M. Bäumer, J. Libuda, and H.-J. Freund, Surf. Sci. **327**, 321 (1995).
[10] E. Durgun, S. Dag, V. M. K. Bagci, O. Gülseren, T. Yildirim, and S. Ciraci, Phys. Rev. B **67**, 201401(R) (2003); S. Dag, E. Durgun, and S. Ciraci, *ibid.* **69**, 121407(R) (2004).
[11] S. B. Fagan, R. Mota, A. J. R. da Silva, and A. Fazzio, Phys. Rev. B **67**, 205414 (2003); J. Phys.: Condens. Matter **16**, 3647 (2004).
[12] Y. Yagi, T. M. Briere, M. H. F. Sluiter, V. Kumar, A. A. Farajian, and Y. Kawazoe, Phys. Rev. B **69**, 075414 (2004).
[13] A. Rubio, J. L. Corkill, and M. L. Cohen, Phys. Rev. B **49**, R5081 (1994).
[14] Y. Miyamoto, A. Rubio, M. L. Cohen, and S. G. Louie, Phys. Rev. B **50**, 4976 (1994).
[15] Y. Miyamoto, A. Rubio, S. G. Louie, and M. L. Cohen, Phys. Rev. B **50**, 18360 (1994).
[16] Z. Weng-Sieh, K. Cherrey, N. G. Chopra, X. Blase, Y. Miyamoto, A. Rubio, M. L. Cohen, S. G. Louie, A. Zettl, and R. Gronsky, Phys. Rev. B **51**, 11229 (1995).
[17] P. Zhang and V. H. Crespi, Phys. Rev. Lett. **89**, 056403 (2002).
[18] H. T. Hall and L. A. Compton, Inorg. Chem. **4**, 1213 (1965).
[19] G. Kresse and J. Furthmüller, Comput. Mater. Sci. **6**, 15 (1996).
[20] G. Kresse and J. Furthmüller, Phys. Rev. B **54**, 11169 (1996).
[21] D. Vanderbilt, Phys. Rev. B **41**, R7892 (1990).
[22] J. P. Perdew and Y. Wang, Phys. Rev. B **45**, 13244 (1992).
[23] H. J. Monkhorst and J. D. Pack, Phys. Rev. B **13**, 5188 (1976).
[24] The buckling of a bond is defined as the difference between the outward extension of one atom and the inward relaxation of the other relative to the average radius of the tube.